Environmental Modelling and Software 164 (2023) 105710

Contents lists available at ScienceDirect

Environmental Modelling and Software

journal homepage: www.elsevier.com/locate/envsoft

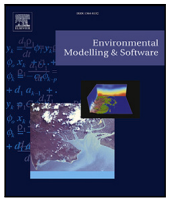

Validating the effect of fuel moisture content by a multivalued operator in a simplified physical fire spread model

M.I. Asensio [a,b,*], J.M. Cascón [a,c], P. Laiz [d], D. Prieto-Herráez [e]

[a] Universidad de Salamanca, University Institute of Fundamental Physics and Mathematics, Plaza de la Merced 4, Salamanca, 37008, Spain
[b] Universidad de Salamanca, Department of Applied Mathematics, Calle del Parque 2, Salamanca, 37008, Spain
[c] Universidad de Salamanca, Department of Economy and Economic History, Edificio FES, Campus Miguel de Unamuno, Salamanca, 37007, Spain
[d] Tecnologías y Servicios Agrarios S.A., S.M.E., M.P. (TRAGSATEC), Rural Development and Forestry Policy Management, Calle Maldonado 58, Madrid, 28006, Spain
[e] Universidad Católica de Ávila (UCAV), Calle Canteros s/n, Ávila, 05005, Spain

ARTICLE INFO

Keywords:
Fuel moisture content
Rate of spread
Multivalued operator
Wildfire spread simulation

ABSTRACT

Fuel moisture content (FMC) plays a significant role in wildfire behavior and rate of spread (ROS). In addition, FMC is a highly dynamic factor and very vulnerable to climate variations. Understanding the effect of FMC on the behavior of fire spread models is crucial, and detailed analysis of specific aspects of complex models is a very effective way to improve them. The simplified physical fire spread model PhyFire considers the effect of FMC in a novel way, involving a multivalued maximal monotone operator. Several numerical experiments have been carried out to confirm that the behavior of the ROS simulated with PhyFire involving FMC is as expected in the reviewed literature: an exponential decrease in fire ROS compared to FMC, for different scenarios, considering different fuel types, terrain slopes and wind speeds. PhyFire performs very accurately, proving that the multivalued operator used is suitable and consistent.

1. Introduction

Fuel moisture content (FMC), defined as the mass of water contained within vegetation in relation to the dry mass, plays a significant role in wildfire behavior and rate of spread (ROS) (Chuvieco et al., 2009). In addition, FMC is one of the most dynamic component of wildfire fuels, it varies rapidly in time and space and it is very vulnerable to weather changes, including air temperature, relative humidity and precipitation (Ellis et al., 2022). Understanding the effect of FMC on fire occurrence and behavior is critical in future climate change scenarios, especially in vulnerable areas as the European Mediterranean Basin (Vilar et al., 2021). FMC is usually separated into dead (DFMC) and live (LFMC) components. Most studies focus on DFMC to understand the effect of FMC on fire spread behavior, as it is easier to reproduce in laboratory experiments. LFMC also affects the flammability of plants, but it is more complex and difficult to quantify this effect. FMC is one of the primary variables in many fire behavior prediction models and fire danger indices. The current capacity to measure FMC remotely (Yebra et al., 2013; Quan et al., 2017) makes it an accessible variable for use in fire behavior models. Therefore, any spread model should suitably capture the effect of FMC on ROS. This paper sets out to prove that the simplified physical fire spread model PhyFire developed by the authors accurately reflects the effect of FMC on the ROS of simulated fires, both separately and in the presence of wind and a terrain slope, for different fuel types. Accordingly, the literature on this effect has been extensively reviewed, with a thorough exploration of experimental studies on the subject. A brief description of PhyFire is accompanied by a particular emphasis on how PhyFire considers FMC, involving a multivalued maximal monotone operator, which is the main novelty of this model compared to others in terms of how to represent the effect of FMC. We also briefly present the latest improvements regarding the numerical resolution of the model. PhyFire is part of a wildfire simulation tool integrated into a geographic information system (GIS), which includes its own wind field simulation model, HDWind. It is not our intention here to provide a detailed description of the two models or of the simulation tool developed accordingly. Numerous aspects of the PhyFire and HDWind models, their numerical implementation, and the GIS tool are described elsewhere (Ferragut et al., 2015, 2011; Prieto et al., 2017; Asensio et al., 2021). Moreover, the PhyFire-HDWind system is a work in progress. We are continuing with the ongoing task of improving the physical models, their numerical implementation

* Corresponding author at: Universidad de Salamanca, University Institute of Fundamental Physics and Mathematics, Plaza de la Merced 4, Salamanca, 37008, Spain.
E-mail addresses: mas@usal.es (M.I. Asensio), casbar@usal.es (J.M. Cascón), plaiz@tragsa.es (P. Laiz), diego.prieto@ucavila.es (D. Prieto-Herráez).

https://doi.org/10.1016/j.envsoft.2023.105710
Received 4 February 2023; Received in revised form 11 April 2023; Accepted 20 April 2023
Available online 27 April 2023

schemes, and their GIS integration. Several numerical experiments have been conducted to confirm that the behavior of the ROS simulated with PhyFire involving FMC is as expected in the reviewed literature in different scenarios (terrain slope, wind speed, and fuel type); in other words, it corresponds to an exponential function in decline, where there is a coefficient k of decay of the curve that explains the effect of moisture. The experiments have been performed using the fire behavior data of forest fuels in the Spanish region of Galicia shown in the photo-guide (Arellano et al., 2016).

2. Model description

Understanding the behavior of a system as complex as a wildfire is an undeniably useful tool for wildfire management, and the development of simulation models plays a key role in this complex challenge (Cardil et al., 2021). There are a large number of models (Sullivan, 2009a,b) and operational tools (Papadopoulos and Pavlidou, 2011) designed for the prediction of wildfire behavior: empirical models (Group, 1992), quasi-empirical models (Rothermel, 1972; Lopes et al., 2002) and physical-based models (Mell et al., 2007), the more complex atmosphere–wildfire coupled models (Mandel et al., 2011), and the recent data-driven or data-assimilation models (Yoo and Song, 2023).

The PhyFire-HDWind operational tool is a GIS-integrated wildfire spread simulation tool developed by the research group on Numerical Simulation and Scientific Computation at the University of Salamanca (Prieto et al., 2017). It is based on the simplified physical fire spread model, PhyFire, and the high-definition wind field model, HDWind. The PhyFire-HDWind code is implemented in C++ using the own Finite Element library Neptuno++ (Cascón et al., 2018), and the API OpenMP for the multiprocessor platforms to reduce computational time (Álvarez et al., 2017). Both models are compatible with any platform and can operate either together or separately. The GIS-integrated PhyFire-HDWind tool was integrated into a web platform: http://sinumcc.usal.es/. This platform was developed using the latest communication and data processing technologies, such as API REST, JSON, and ArcGIS Server (Asensio et al., 2021). This open-access system enables any Internet user to use the PhyFire-HDWind tools without any prior knowledge of either the models or the GIS tools. The system carries out all the steps of the simulation process in a holistic manner, providing the user with a rapid display of the simulation results. The advantages of PhyFire's technological improvements do not obviate the key question of model reliability. The aim here is to further our understanding of the model's performance regarding FMC, and find out if it responds as expected in several scenarios, including different fuel types, wind speeds and terrain slopes. We will therefore restrict ourselves to the PhyFire model, with particular emphasis on the effect of humidity through a multivalued operator. In addition, the experiments here use a constant wind speed, so the HDWind model is not used, except in the real example in Section 6. No further details on this model are included here, but they can be found in Asensio et al. (2005), Ferragut et al. (2011, 2013) and more recently in Prieto-Herráez et al. (2021).

2.1. The fire model: PhyFire

PhyFire is a simplified two-dimensional one-phase physical fire spread model based on energy and mass conservation equations (Asensio et al., 2021). This model considers convection and radiation as dominant thermal transfer mechanisms (Morvan, 2011), and depends mainly on meteorological data (wind direction and intensity, ambient temperature, and humidity), topography, and fuel type and load. To better understand the PhyFire model, we briefly present and explain the equations of the current version of the model as well as the last numerical scheme used to solve it (Asensio et al., 2023), focusing on the multivalued function representing the effect of the FMC. The equations of the PhyFire model are as follows,

$$\partial_t e + \beta \mathbf{v}\cdot\boldsymbol{\nabla} e + \alpha u = r(u,c) \quad \text{in } S\times(0,t_{max}) \tag{1}$$

$$e \in G(u) \quad \text{in } S\times(0,t_{max}) \tag{2}$$

$$\partial_t c = -g(u)\,c \quad \text{in } S\times(0,t_{max}) \tag{3}$$

where the unknowns are the dimensionless enthalpy $e = E/MCT_\infty$, the dimensionless solid fuel temperature $u = (T - T_\infty)/T_\infty$, and the solid fuel mass fraction $c = M/M_0$, defined on the surface S where the fire develops. The physical quantities E (J m^{-2}), T (K), and M (kg m^{-2}) are enthalpy, the temperature of the solid fuel, and the fuel load, respectively, and C (J K^{-1} kg^{-1}) is the heat capacity of the solid fuel, T_∞ (K) is a reference temperature, and M_0 (kg m^{-2}) is the initial solid fuel load.

Surface S is defined by the mapping

$$S : d \longmapsto \mathbb{R}^3$$
$$(x,y) \longmapsto (x,y,h(x,y))$$

where $h(x,y)$ is a known function representing the topography of the surface S, and $d = [0,l_x]\times[0,l_y] \subset \mathbb{R}^2$ is a rectangle representing the projection of the surface S.

Fuel is described by the given initial fuel load M_0 and the moisture content M_v (kg of water/kg of dry fuel), as well as the fuel type, which are scalar functions defined on d. Fuel type determines the value of some input variables of the model as shown in Table 1.

We use homogeneous Dirichlet *boundary conditions*, whereby the model is valid as long as the fire does not reach the boundary. The *initial conditions* represent the value of the nondimensional solid fuel load, including eventual fire breaks, and the source of the fire. PhyFire allows restarting the simulation using intermediate fire perimeters with updated meteorological information.

The term $r(u,c)$ on the right-hand side of Eq. (1) represents the energy due to radiation and depends on the radiation absorption coefficient inside the flame, a, the first of the three model parameters listed in Table 1 that should be adjusted. Thermal radiation has a significant effect on ROS, drying the fuel at the fire's leading edge, and thus accelerating its ignition. The radiation term is highly nonlinear and three-dimensional, so the computational cost of its numerical solution in wildfire spread models makes it a challenging task. When the flame is not vertical due to wind or terrain slope, the effect of thermal radiation is higher downwind and upslope, respectively. To deal with this effect, radiation is represented by a non-local radiation term, solving the corresponding radiation intensity equation in a three-dimensional domain representing the air layer D over surface S,

$$D = \{(x,y,z) : (x,y)\in d, h(x,y) < z < h(x,y)+\delta\}$$

where δ is the height of the air layer assuming that the height of the flames is always less than δ. For more details about how to solve the differential equation representing the radiation intensity and how to compute incident radiation energy at each point on the surface S see Ferragut et al. (2015). Notice note that the flame geometry affects the radiation received at each point, so in the computation of the radiation detailed in the previous reference it is distinguished whether the flame is vertical or tilted.

As mentioned above, in this paper we pay particular attention to how the PhyFire model addresses the effect of the FMC. The influence of FMC and heat absorption by pyrolysis is handled by a multivalued maximal monotone operator representing enthalpy (Ferragut et al., 2007) in Eq. (2). As far as we know, PhyFire is the first and only fire spread model that treats the enthalpy equation with a multivalued operator, defined as follow,

$$G(u) = \begin{cases} u & \text{if} \quad u < u_v, \\ [u_v\ ,\ u_v+\lambda_v] & \text{if} \quad u = u_v, \\ u+\lambda_v & \text{if} \quad u_v < u < u_p, \\ [u_p+\lambda_v\ ,\ \infty] & \text{if} \quad u = u_p, \end{cases} \tag{4}$$

where u_v and u_p are the non-dimensional evaporation temperature of the water and the non-dimensional pyrolysis temperature of the solid fuel, respectively. FMC, denoted in the model equations by M_v (kg of water/kg of dry fuel), appears in the multivalued operator through λ_v, which is the non-dimensional evaporation heat,

$$\lambda_v = \frac{M_v \Lambda_v}{C T_\infty}$$

where $\Lambda_v = 2.25 \times 10^6$ (J kg^{-1}) is the latent heat of evaporation of water. It should be noted that in the burned area $\lambda_v = 0$. The use of a multivalued operator is informed by the classical two-phase Stefan problem, and it has been adapted to model the two well-defined phases in a wildfire combustion process (Cox, 1995): the endothermic phase that includes the dehydration of the solid fuel, and the exothermic phase in which the flammable mixture from fuel pyrolysis begins to release energy. These are the solid and gaseous phase, respectively, which in PhyFire are simplified by the multivalued operator G, the correction factor β in the convective term of Eq. (1), and flame temperature and height in the radiation term.

Flame height depends on wind strength and surface slope (Asensio-Sevilla et al., 2020). PhyFire has been provided with a flame height sub-model depending on these two factors, based on the observation of the experimental curves for different fuels (Arellano et al., 2016). The flame height sub-model is as follows:

$$F = (F_H + F_v\ |v|^{(1/2)})(1 + F_s s^2) \tag{5}$$

where F_H is an independent flame-height parameter, F_v is a wind correction factor, F_s is a slope correction factor, $|v|$ is the wind strength in m/s, and s represents the slope at each point on the surface, providing a flame height in meters.

Flame temperature is approximated in terms of solid fuel under some simplifications. We assumed that this temperature does not vary inside a stabilized flame, that heat losses inside the flame are mainly due to local radiation, and that a maximum flame temperature $T_{f,max}$ is available. In Asensio et al. (2023) can be found the details of how to derive the following expression for flame temperature,

$$T_f = (T_\infty^4 + (t > t_p)(T_{f,max}^4 - T_\infty^4)M)^{1/4} \tag{6}$$

where the term $(t > t_p)$ is zero when the process is endothermic, and one, when it is exothermic.

The other major heat transfer mechanism in a wildfire is convection, which is represented in PhyFire through the convective term $\beta v \cdot \nabla e$ in Eq. (1). This term represents the energy convected by the gas pyrolyzed through the elementary control volume, where the non-dimensional surface wind speed v can either be a constant value or variable both spatially and temporally, for example, provided by the high definition HDWind model. The correction factor β represents the fraction of transported enthalpy retained by the solid fuel in the aforementioned one-phase simplification. β is the second of the three model parameters that should be adjusted. For further details about parameter β, see Prieto et al. (2015).

As regards the other terms, αu represents the energy lost by natural vertical convection, where α is the non-dimensional coefficient, that depends on the natural convection coefficient H, the third model parameter to be adjusted.

The right-hand side of Eq. (3) represents the loss of solid fuel due to combustion, assuming there is no loss below the pyrolysis temperature and that the loss rate remains constant when this temperature is reached. This rate is inversely proportional to the solid half-life time $t_{1/2}$ of the combustion of each type of fuel.

Eqs. (1), (2), (3) properly reflects the simplified combustion process in the burning area, but these equations can be further simplified in the burned area, assuming that once the fuel has been burned the enthalpy is not recovered, and considering that an area is fully burned when the mass fraction of solid fuel is less than 0.1. Then the only equation to be solved in the burned area is

$$\partial_t u + \alpha u = r(u, c) \qquad \text{in } S \times (0, t_{max}) \tag{7}$$

where we are neglecting the heat transported by convection to the burned area.

Table 1
PhyFire input variables and parameters, with their symbols and units.

Fuel-type-dependent input variables	Symbol	Units
Heat capacity	C	J K^{-1} kg^{-1}
Pyrolysis temperature	T_p	K
Flame temperature	T_f	K
Combustion half-life time	$t_{1/2}$	s
Maximum fuel load	M_0	kg m^{-2}
Moisture content	M_v	$\frac{\text{kg}(water)}{\text{kg}(dry\ fuel)}$
Flame height factor	F_H	m
Wind correction factor	F_v	m$^{1/2}$ s$^{1/2}$
Slope correction factor	F_s	–
Environmental input variables	**Symbol**	**Units**
Non-dimensional wind speed	v	–
Reference temperature	T_∞	K
Height of the surface	h	m
Fuel load	M	kg m^{-2}
Model parameters	**Symbol**	**Units**
Mean absorption coefficient	a	m^{-1}
Natural convection coefficient	H	J s^{-1} m^{-2} K^{-1}
Convective term correction factor	β	–

2.2. Numerical method

The numerical method used to solve this non-local radiation model included a P1 finite element method for the spatial discretization on a regular mesh, combined with a predictor–corrector finite difference scheme for the time discretization. The predictor step is a Euler semi-implicit scheme, and the corrector step is a modified Crank–Nicolson scheme. After analyzing other numerical schemes throughout the development process of the PhyFire model, its numerical resolution and its practical implementation (see Asensio et al. (2023)), this scheme has provided stable numerical solutions and a good balance between efficiency and computational cost. The computational cost has been reduced by defining what we define as *Active Nodes*, so that the equations are solved only in the neighborhood of the fire front, and by adapting the numerical scheme and the corresponding code to parallel computing (Ferragut et al., 2015). The spatial discretization varies depending on the precision level, currently varies from precision level 0 corresponding to 50 m cell size, to precision level 5, corresponding to 2.5 m cell size. For the experiments performed in this work we have used precision level 4 (5 m cell size) for the study of the behavior of ROS versus FMC in Section 4.4, and precision level 3 (7.5 m cell size) for the simulation of the real case in Section 6.

Given the initial values u^0 and c^0 defined by the initial conditions, we set the value of the initial enthalpy for each node i of the spatial discretization depending on the initial nondimensional temperature u^0 as follow,

$$e_i^0 = \begin{cases} u_i^0 & \text{if} \quad u_i^0 \le u_v, \\ u_i^0 + \lambda_v & \text{if} \quad u_i^0 > u_v, \end{cases} \tag{8}$$

Given the values of the unknowns u^n, c^n and e^n at time step n, we compute u^{n+1}, c^{n+1} and e^{n+1} by means of the following steps,

1. Build the set of *Active Nodes*.
2. Compute the *Radiation Heat*.
3. *Prediction step*: Semi-implicit Euler method.
4. Update the set of *Active Nodes*.
5. Update the *Radiation Heat*.

6. *Correction Step*: Modified Crank–Nicolson method.

A node i is considered an *Active Node* if $u_i > 0$ and $c_i \geq 0.1$ or if it belongs to the *Radiation molecule* associated to a node fulfilling the previous condition. The *Radiation molecule* is a set of nodes consisting of the node itself and the neighboring nodes defining the area affected by the radiation emitted by the node in question

The numerical computation of the radiation term for each time step r^n is fully described in Ferragut et al. (2015), we focus here on those numerical aspects of the algorithm that are new compared to previous versions, specifically the predictor–corrector finite difference scheme.

We must first mention the total discretization of the convective term of Eq. (1) that is carried out in each step of the predictor–corrector scheme,

$$\partial_t e + \beta \mathbf{v}.\nabla e \approx \frac{1}{\Delta t}(e^{n+1} - \bar{e}^n)$$

where $\bar{e}^n = e^n \circ X^n$, and $X^n(\mathbf{x}) = X(\mathbf{x}, t^{n+1}, t^n) \approx \mathbf{x} - \beta \mathbf{v} \Delta t$ is the position at time t^n of the particle that is at position $\mathbf{x}$ at time t^{n+1}.

Predictor step. The discrete equations in the *burning area* in the predictor step correspond to a semi-implicit Euler scheme,

$$\frac{e^{n+1/2} - \bar{e}^n}{\Delta t} + \alpha u^{n+1/2} = r^n, \tag{9}$$

$$e^{n+1/2} \in G(u^{n+1/2}), \tag{10}$$

$$\frac{c^{n+1/2} - c^n}{\Delta t} = -g(u^{n+1/2}) c^{n+1}. \tag{11}$$

where $e^{n+1/2}$, $u^{n+1/2}$ and $c^{n+1/2}$ stand for the predicted value of e^{n+1}, u^{n+1} and c^{n+1} respectively. The basic idea is to handle the linear term implicitly, and since the non-local radiation term r^n depends strongly on the temperature u^n and on the solid fuel c^n, they are evaluated explicitly at time t^n. But even so, Eqs. (9)–(11) continue to be non-linear due to the multivalued operator G. Nevertheless, the solution of this problem can be reduced to explicit calculations.

The multivalued operator in Eq. (10) is maximal monotone and hence its resolvent $J_\mu = (Id + \mu G)^{-1}$ is a well defined univalued operator for any $\mu > 0$. Moreover, the Yosida approximation (Bermúdez and Moreno, 1981) of G, $G_\mu = \frac{Id - J_\mu}{\mu}$ is a Lipschitz operator and the inclusion in Eq. (10) is equivalent for all $\mu > 0$ to the following equation

$$e^{n+1/2} = G_\mu(u^{n+1/2} + \mu e^{n+1/2}), \tag{12}$$

or

$$u^{n+1/2} = J_\mu(u^{n+1/2} + \mu e^{n+1/2}). \tag{13}$$

Now rearranging Eq. (9)

$$u^{n+1/2} + \frac{1}{\alpha \Delta t} e^{n+1/2} = \frac{1}{\alpha \Delta t} \bar{e}^n + \frac{1}{\alpha} r^n. \tag{14}$$

and taking $\mu = 1/(\alpha \Delta \tau)$ in Eq. (13), we obtain

$$u^{n+1/2} = J_{1/\alpha \Delta t}\left(\frac{1}{\alpha \Delta t} \bar{e}^n + \frac{1}{\alpha} r^n\right) \tag{15}$$

which it is equivalent to solve

$$(\alpha \Delta t\ Id + G) u^{n+1/2} \ni \bar{e}^n + \Delta t\ r^n. \tag{16}$$

Thus, denoting $æ^n = \bar{e}^n + \Delta t\ r^n$, the value of $u^{n+1/2}$ is given by,

$$\begin{aligned}
&\frac{æ^n}{1+\alpha \Delta t} && \text{if} \quad æ^n < (1+\alpha \Delta t)\, u_v,\\
&u_v && \text{if} \quad æ^n \in [(1+\alpha \Delta t)\, u_v, (1+\alpha \Delta t)\, u_v + \lambda_v],\\
&\frac{æ^n - \lambda_v}{1+\alpha \Delta t} && \text{if} \quad æ^n \in [(1+\alpha \Delta t)\, u_v + \lambda_v, (1+\alpha \Delta t)\, u_p + \lambda_v],\\
&u_p && \text{if} \quad æ^n \in [(1+\alpha \Delta t)\, u_p + \lambda_v, \infty].
\end{aligned} \tag{17}$$

Once $u^{n+1/2}$ has been obtained, we calculate $e^{n+1/2}$ and $c^{n+1/2}$ explicitly from Eq. (9) and (11) respectively,

$$e^{n+1/2} = \bar{e}^n - \alpha \Delta t u^{n+1/2} + \Delta t\, r^n, \tag{18}$$

$$c^{n+1/2} = \frac{c^n}{1 + \Delta t g(u^{n+1/2})}. \tag{19}$$

Notice that Eqs. (15), (18) and (19) can be solved simultaneously in all *Active Nodes*, so parallel computation can be used to reduce the computational cost. Indeed, the loop over all *Actives Nodes* to compute $u^{n+1/2}$, $e^{n+1/2}$ and $c^{n+1/2}$ has been parallelized using the API OpenMP (Chapman et al., 2007).

In the *burned area*, only Eq. (7) needs to be solved, whose discrete version using a semi-implicit Euler scheme is,

$$\frac{u^{n+1/2} - u^n}{\Delta t} + \alpha u^{n+1/2} = r^n \tag{20}$$

that can be solved explicitly,

$$u^{n+1/2} = \frac{u^n + \Delta t\, r^n}{1 + \alpha \Delta t} \tag{21}$$

Corrector step. The discrete equations in the *burning area* in the corrector step correspond to a Crank–Nicolson scheme,

$$\frac{e^{n+1} - \bar{e}^n}{\Delta t} + \alpha \frac{u^{n+1} + u^n}{2} = \frac{r^{n+1/2} + r^n}{2} \tag{22}$$

$$e^{n+1} \in G(u^{n+1}), \tag{23}$$

$$\frac{c^{n+1} - c^n}{\Delta \tau} = -g\left(\frac{u^{n+1} + u^n}{2}\right) \frac{c^{n+1} + c^n}{2} \tag{24}$$

where we have approximate r^{n+1} by $r^{n+1/2}$ computed in terms of $u^{n+1/2}$ and $c^{n+1/2}$, the estimations obtained in the prediction steps, as at this point u^{n+1} and c^{n+1} are not known. As in the prediction step, rearranging Eq. (22), we have,

$$u^{n+1} + \frac{2}{\alpha \Delta t} e^{n+1} = \frac{2}{\alpha \Delta t} \bar{e}^n - u^n + \frac{r^{n+1/2} + r^n}{\alpha}. \tag{25}$$

As in the predictor step, taking $\mu = \frac{2}{\alpha \Delta t}$, the multivalued Eq. (23) can be written as

$$u^{n+1} = J_{\frac{2}{\alpha \Delta t}}\left(\frac{2}{\alpha \Delta t} \bar{e}^n - u^n + \frac{r^{n+1/2} + r^n}{\alpha}\right) \tag{26}$$

which it is equivalent to solve

$$\left(\frac{2}{\alpha \Delta \tau} Id + G\right) u^{n+1} \ni \left(\frac{2}{\alpha \Delta t} \bar{e}^n - u^n + \frac{r^{n+1/2} + r^n}{\alpha}\right). \tag{27}$$

Denoting now $æ^n = \frac{2}{\alpha \Delta t} \bar{e}^n - u^n + \frac{r^{n+1/2} + r^n}{\alpha}$, the value of u^{n+1} is given by,

$$\begin{aligned}
&\frac{æ^n}{1+\frac{\alpha \Delta t}{2}} && \text{if} \quad æ^n < (1+\frac{\alpha \Delta t}{2})\, u_v,\\
&u_v && \text{if} \quad æ^n \in [(1+\frac{\alpha \Delta t}{2})\, u_v, (1+\frac{\alpha \Delta t}{2})\, u_v + \lambda_v],\\
&\frac{æ^n - \lambda_v}{1+\frac{\alpha \Delta t}{2}} && \text{if} \quad æ^n \in [(1+\frac{\alpha \Delta t}{2})\, u_v + \lambda_v, (1+\frac{\alpha \Delta t}{2})\, u_p + \lambda_v],\\
&u_p && \text{if} \quad æ^n \in [(1+\frac{\alpha \Delta t}{2})\, u_p + \lambda_v, \infty].
\end{aligned} \tag{28}$$

Again, once u^{n+1} has been obtained, we can update the enthalpy e^{n+1} from Eq. (22), and the fuel c^{n+1} from Eq. (24),

$$e^{n+1} = e^n - \alpha \Delta t \frac{u^{n+1} + u^n}{2} + \Delta t \frac{r^{n+1/2} + r^n}{2}, \tag{29}$$

$$c^{n+1} = \frac{1 - \frac{\Delta t}{2} g(\frac{u^{n+1} + u^n}{2})}{1 + \frac{\Delta t}{2} g(\frac{u^{n+1} + u^n}{2})} c^n. \tag{30}$$

Once more, Eqs. (26), (29) and (30) can be solved simultaneously in all *Active Nodes*, so again the parallel calculation allows us to reduce the computational cost in the correction step.

In the *burned area*, only (22) needs to be considered, which can be solved explicitly,

$$u^{n+1} = \frac{(1 - \frac{\alpha \Delta t}{2}) u^n + \frac{\Delta \tau}{2}(r^{n+1/2} + r^n)}{1 + \frac{\alpha \Delta t}{2}}$$

Table 2
Literature review of k coefficient values relating ROS and FMC through Eq. (31). ROS: rate of spread; FMC: weighted fuel moisture content according to the proportion of live and dead fuel load; FMC_{dead}: fuel moisture content of dead fuel; FMC_{live}: fuel moisture content of live fuel.

Ref.	Experiment type	k coeff.	FMC (%)	Fuel type	Wind (km h^{-1})
Cheney et al. (1993)	Field	0.0966	2.7–12.1	Grassland	7-25
Burrows (1999)	Field	0.120 0.160 0.190 0.340 0.330	3.0-18.6	Litter bed of dead leaves, twigs and bark of Eucalyptus marginata	2.0-3.5 3.5-4.5 4.5-5.5 5.5-6.5 6.5
Fernandes et al. (2009)	Field	0.039 0.040	3.7–41.7 8.4–41.5	Dead needles of Pinus pinaster	Head fires 0.5-22 Back fires 0.5-23.1
Marino et al. (2012)	Outdoor wind tunnel burns	0.17	FMC_{dead}: 22–36 FMC_{live}: 49–84 FMC_{dead}: 20–34 FMC_{live}: 65–105 FMC_{dead}: 10–20 FMC_{live}: 15–113	Erica, Ulex and Pterospartum Ulex europaeus Ulex europaeus	8.3 8.3 12.6
Anderson et al. (2015)	Prescribed fires and wildfires	0.0761 0.0762 0.0721	FMC_{dead}: 2-30 FMC_{live}: 58-236	Shrubland	4-25
Anderson et al. (2015)	Prescribed fires and wildfires	0.0761 0.0762 0.0721	FMC_{dead}: 2-30 FMC_{live}: 58-236	Shrubland	4-25
Rossa et al. (2016)	Laboratory	0.0117 0.0059 0.0122 0.0089 0.0063	12.9–110.8 25.5–179.3 18.3–145.9 12.9–179.3 >50	Acacia Dealbata Cytisus striatus Eucalyptus globulus All fuel types All fuel types	1.5

3. Fuel moisture content as a wildfire spread factor

FMC has a direct relationship with wildfire ROS, being one of the variables together with wind that most influences it (Chuvieco et al., 2009), mainly through the process of heating and subsequently evaporating the water in the fuel, enabling it to attain combustion conditions. This process involves the consumption of the energy released by the adjacent combustion fuel, and requires time, which reduces ROS as moisture increases.

The laboratory and field fires analyzed in Rossa and Fernandes (2018b) have evidenced that wind explains 61.9% of ROS variance, while DFMC explains the remaining 38.1%. Furthermore, the damping effect of moisture on ROS is not affected by the wind, remaining constant (Rossa and Fernandes, 2017).

There is consensus on the crucial influence that DFMC has on ROS, but there are discrepancies over the influence of LFMC (Finney et al., 2013), which are manifested in theoretical propagation models (Rothermel, 1972; Albini, 1976; Stocks et al., 1989), and are based on experimental trials. Contradictory results are obtained between field tests involving controlled burning, where LFMC barely influences ROS, and laboratory studies, in which there is a clear relationship between LFMC and ROS (Rossa and Fernandes, 2018b).

Consequently, propagation models based on laboratory studies often use a weight of live and dead fuel based on their mass, while those informed by field experiments consider only dead fuel (Rossa and Fernandes, 2018b).

This difficulty in detecting the influence of live fuel on ROS in field tests is because it can be concealed in two different ways: on the one hand, live fuel maintains an almost constant moisture content throughout the year (e.g., mature pine needles, or other fuels in non-Mediterranean climates), or on the other, their variation follows a similar pattern to that of dead fuel (measured as a monthly average). Many models are therefore based solely on dead fuel, but it should be noted that this is only true if the moisture implicit in the live fuel (albeit not accounted for) remains within the same ranges as during the experimentation informing the model. If, for example, FMC is much lower due to drought, the model will no longer hold (Rossa and Fernandes, 2018a), and will even pose a threat if used in prevention/extinction operations. Experiments carried out in the laboratory using a mix of live and dead fuel seem to confirm that LFMC reduces ROS in the same proportion as dead fuel, without finding any significant differences between the two (Marino et al., 2012; Rossa and Fernandes, 2017). The decisive variable is therefore the moisture content weighted according to mass (in dry weight), regardless of whether it is alive or dead. Moreover, live and dead fuels influence ROS through the same mechanism; that is, through the absorption of the heat generated by the fire to raise its temperature and subsequently evaporate before the fuel can begin to burn. This means the phenological state of the vegetation is not relevant, but instead its moisture content (Rossa and Fernandes, 2017). There are indications, however, that the ignition mechanism of live fuel may be different, as it may ignite before all the water content has evaporated (Finney et al., 2013; Rossa and Fernandes, 2018a). After conducting a series of laboratory experiments with live fuel involving four common mountain species in Portugal, (Rossa et al., 2016) conclude that there is a threshold for LFMC of between 50% and 70% (although in another paper they report 100%, (Rossa and Fernandes, 2017)), whereby the influence the increase has on ROS is small (although present), which is consistent with field observations. Viegas et al. (2013) report a threshold in the proportion of dead fuel to live one below which the fire stops spreading (ROS = 0). This value depends on the moisture content of both types of fuel and environmental conditions.

To explain the influence of FMC on ROS, several authors (Cheney et al., 1993; Burrows, 1999; Fernandes et al., 2009; Marino et al., 2012; Anderson et al., 2015; Rossa et al., 2016) use an exponential function in decline, where there is a coefficient k of decay of the curve that explains the effect of moisture in both laboratory and field experiments. The function is as follows,

$$ROS = c\, e^{-k\, FMC} \tag{31}$$

This function is usually integrated as a term into a general function of ROS including other variables, such as wind speed, slope, depth of the fuel bed, or degree of cure of the herbaceous fuel. Table 2 shows coefficient k values for different studies, with k values corresponding mainly to ROS measurements in m min^{-1}.

Table 3
Fuel load, weighted height and flame height coefficients according to flame height Eq. (5) for the five fuel types selected from the photo-guide (Arellano et al., 2016) and the corresponding NFFL classification fuel type. F_H: flame height independent parameter; F_v: wind correction factor; F_s: slope correction factor; R^2: coefficient of determination.

NFFL fuel type	(Arellano class) Main species	Fuel load (kg m^{-2})	Weighted height (m)	Eq. (5) fit (F_H, F_v, F_s)	R^2
1 Short grass	(Ac-01) Agrostis curtisii, Pterospartum tridentatum	1.254	0.14	0.204 0.615 5.449	0.979
4 Chaparral	(Ea-08) Erica australis, Erica arborea, Pterospartum tridentatum	4.907	2.21	2.569 0.911 2.981	0.961
5 Brush	(Ea-01) Erica australis, Pterospartum tridentatum, Halimium alyssoides	1.257	0.45	2.499 0.519 2.798	0.952
6 Dormant brush, hardwood slash	(Es-01) Erica scoparia, Ulex breoganii	1.901	1.03	2.693 0.641 2.908	0.955
7 Southern rough	(Cl-02) Cistus ladanifer	1.456	1.03	2.370 0.637 2.888	0.960

Part of the literature reviewed reports other versions of this exponential relationship, including the effect of wind and terrain slope. Cheney et al. (1993), Burrows (1999), Fernandes et al. (2009), Anderson et al. (2015) propose the following equation,

$$ROS = c\, v^b\, e^{-k\, FMC} \tag{32}$$

where v is surface wind speed.

Marino et al. (2012) propose a linear model for wind, as their experimental study is limited to two wind figures, but they stress that this model has no predictive value for wind effect. This study is of particular interest because it compares experimental data and predictions from the physically-based model FIRETEC, as in this article with PhyFire. One of the problems mentioned in Marino et al. (2012) is the difference in scale between experiments and simulations with FIRETEC. This is not an issue in our study, as PhyFire allows computations at different scales by changing the precision level.

Other authors also suggest that the impact of FMC upon the fire behavior was also affected by the wind conditions and substantiate this with numerical experiments (Morvan, 2013), but do not propose a particular expression of this relationship.

The model suggested in Fernandes et al. (2009) describes ROS in terms of surface wind speed and FMC, and also slope terrain (s), through the following function,

$$ROS = c\, v^b\, e^{p\, s - k\, FMC} \tag{33}$$

4. Methodology

4.1. Description of the experiments

The spatial domain for the experiments is an even sloping surface with a manageable but realistic scale, namely, 6000 m × 3000 m. The fire focus is a line 25 m wide located at a distance of 1000 m from the lower short side. Wind and slope are taken in the same direction, that is, the fire front follows both the slope and the wind.

ROS is computed as the slope of the linear regression line used to fit the position of the fire front in real time every five minutes from minute 10 to minute 60, measured lengthwise. The ROS calculation code provides controls to detect if the fire goes out or if it is approaching the limit of the domain, avoiding unnecessary or unrealistic calculations.

Uniform fuel distribution is considered for four types of brush and one type of grass selected from the comprehensive report (Arellano et al., 2016). This is a photo-guide that provides valuable information about the main forestry fuels in Galicia, in northwest Spain, and specifically the main physical features of fuels related to their fire behavior, which are of particular interest to this study. This guide provides a system for estimating the probable behavior of a wildfire that involves the fuels analyzed, including flame height and ROS under a range of scenarios: three different slopes (0%, 20%, and 40%) and wind speed ranging between 0 and 60 km h^{-1}. There is also information on the fuel load and its weighted height. These data have allowed us to adjust the parameters and certain input variables in PhyFire.

Table 3 lists some of the properties of the five fuels selected: the model corresponding to one of the 13 standard fuels according to the Northern Forest Fire Laboratory (NFFL) classification system (Anderson, 1982), the specific fuel from the photo-guide (Arellano et al., 2016), and certain characteristics such as fuel load or weighted height.

4.2. Flame height adjustment

The first step involved adjusting the flame height sub-model coefficients in Eq. (5) for each one of the five fuel types selected by a nonlinear least square approximation of flame height data obtained from graphics in the photo-guide (Arellano et al., 2016) for different slopes (0%, 20%, and 40%) and wind speed at intervals of 5 km h^{-1} from 0 to 45 km h^{-1}. As regards the four types of brush, flame height data for a wind speed of 0 km h^{-1} was not considered due to its high uncertainty. Conversely, grassland analyzed in Arellano et al. (2016) report that the fire does not spread in conditions of no wind and no slope, and flame height is zero, so these flame height data should be included. The adjustment has been performed using CFTool, the MatLab Curve Fitting Toolbox, selecting a Levenberg–Marquardt algorithm, reaching a coefficient of determination $R^2 > 0.95$ in all cases. Table 3 contains the flame height model coefficients computed, and the goodness of fit in terms of the coefficients of determination R^2. The goodness of flame height sub-model Eq. (5) has been discussed in detail in Asensio-Sevilla et al. (2020), so here we only provide the value of the coefficient of determination R^2 to justify the adjustment, without specifying other error metrics, as this is not the aim of this study.

4.3. Parameter adjustment

The second step is the adjustment of the three PhyFire parameters, namely, the mean absorption coefficient a; the natural convection coefficient H, and the correction factor of the convective term β, using these five fuel models and ROS data from the photo-guide (Arellano et al., 2016) for the given ranges of wind speed and terrain slope. The initial aim was to follow the same parameter adjustment strategy as in Prieto et al. (2015), where we first adjusted a and H for no wind and no slope fire data, with β then being adjusted with all the other ROS data for the given terrain slopes and wind speeds. This strategy was shown to be effective in Prieto et al. (2015), and responded to

Table 4
Mean absorption coefficient (a) values for all the scenarios.

	Slope	5 km h^{-1}	10 km h^{-1}	15 km h^{-1}	20 km h^{-1}	25 km h^{-1}
Fuel 1	0%	–	0.258	0.319	0.337	0.375
	20%	0.209	0.630	0.715	1.076	1.026
	40%	0.155	0.997	1.609	1.723	4.812
Fuel 4	0%	0.122	0.119	0.084	0.078	0.085
	20%	0.140	0.120	0.135	0.168	0.200
	40%	0.085	0.173	0.224	0.369	0.776
Fuel 5	0%	0.063	0.033	0.021	0.020	0.019
	20%	0.054	0.055	0.049	0.048	0.055
	40%	0.079	0,060	0.065	0.099	0.091
Fuel 6	0%	0.110	0.057	0.071	0.060	0.051
	20%	0.133	0.088	0.089	0.094	0.154
	40%	0.114	0.114	0.145	0.190	0.325
Fuel 7	0%	0.098	0.051	0.063	0.053	0.047
	20%	0.125	0.099	0.080	0.093	0.136
	40%	0.107	0.107	0.135	0.158	0.266

the conclusions derived from the sensitivity analysis and parameter adjustment reported there, where a and H did not vary significantly for different scenarios, including slope, wind, and fuel moisture content, always recording the same order of magnitude. β became the most relevant input factor for ROS, strongly dependent on wind magnitude. This strategy has proven inadequate here due to the incorporation of the new flame height sub-model given by Eq. (5). An in-depth study of the parameter adjustment process revealed an important change in the sensitivity of the model parameters. A new global sensitivity analysis (GSA) of PhyFire parameters showed a major change in the importance of both the mean absorption coefficient a, and the correction factor of convective term β. This new GSA was performed using the SAFE (Sensitivity Analysis For Everybody) MatLab Toolbox (Pianosi et al., 2015) with the Elementary Effect Test (Saltelli et al., 2008). The results of this GSA revealed the greater importance of the mean absorption coefficient a in all scenarios, whereby the flame height sub-model corrects the undue importance of the correction factor of convective term β. Although not the subject of this study, the results of this GSA have been used here to design a better model parameter adjustment strategy. We have fixed H in a previous adjustment using only no wind and no slope ROS data, obtaining a mean value of 10.605 J s^{-1} m^{-2} K^{-1}. β has been selected in the order of hundredths ($\beta = 0.02$), its typical value (Prieto et al., 2015), but with the aim of assuring the existence of an optimum value of the third parameter a in all scenarios. The objective here is to verify whether PhyFire simulations confirm the exponential function (31) assessing the isolated effect of FMC on ROS, as well as functions (32) and (33) when wind speed and terrain slope are considered. It is therefore important to best fit the model to each scenario and choose the scenarios with the least uncertainty among all those previously analyzed. A bisection method has been used to determine the value of the parameter a that equals the value of the computational ROS with the experimental ROS for each scenario. The parameter adjustment has been implemented in C++ as PhyFire in order to optimize the adjustment process, as the evaluation of the model is the costliest part. The total number of cases analyzed amounts to 74, corresponding to the five fuel types, three terrain slopes (0%, 20%, and 40%), and five wind speeds (5, 10, 15, 20, and 25 km h^{-1}), except for grass and 0% slope, where the wind speed of 5 km h^{-1} is not considered. Scenarios with a lower degree of uncertainty have been considered, avoiding very low or very high winds in which the data are less reliable. The results of this adjustment are shown in Table 4.

4.4. Data analysis ROS versus FMC

Once the model parameters have been adjusted for each scenario, each wind speed, terrain slope, and fuel type, PhyFire has been evaluated by varying the FMC to test whether the simulated ROS record an exponential decay as a function of FMC, as in the empirical models reviewed. FMC ranges from 3% to 244%, using 17 values following an exponential distribution, as previous observation of the results showed that high FMC produces few changes in ROS. This is the first positive observation of the good behavior of the PhyFire model in this study: the overall trend in the ROS-FMC relationship suggests an FMC threshold of 50 − 70%, above which its response to increasingly higher FMC is weak (Rossa et al., 2016). Nonlinear regression analyses have been performed to summarize the behavior of ROS for the simulation data in terms of FMC, Eq. (31), FMC and wind speed, Eq. (32), and FMC, wind speed, and terrain slope, Eq. (33), for all the fuel types selected. A routine has been built in MatLab based on the function *lsqcurvefit*, which solves nonlinear curve-fitting (data-fitting) problems in the least-squares sense, selecting the Levenberg–Marquardt algorithm. This MatLab function returns the adjusted parameters, the squared 2-norm of the residual, and the residual array itself. This allows easy calculation of the coefficient of determination (R^2) and an overall indicator of goodness of fit, as well as the adjusted coefficient of determination R^2_{Adj} - a modified version of R^2 for the number of independent variables in the model.

$$R^2 = 1 - \frac{\sum_{i=1}^{n}(y_i - \hat{y}_i)^2}{\sum_{i=1}^{n}(y_i - \bar{y})^2}$$

$$R^2_{Adj} = 1 - \frac{(1 - R^2)(n-1)}{n - (d+1)}$$

Other deviation measures computed to evaluate the model's performances were the root-mean-square error (RMSE) and the mean absolute error (MAE), as well as their normalized versions: the normalized root-mean-square error (NRMSE) and the normalized mean absolute error (NMAE), in order to relate the corresponding error measures to the observed range of the variable. We also provide the mean biased error (MBE) to discover whether the models tend to overestimate or underestimate ROS.

$$RMSE = \sqrt{\frac{1}{n}\sum_{i=1}^{n}(y_i - \hat{y}_i)^2}$$

$$NRMSE = \frac{RMSE}{\bar{y}}$$

$$MAE = \frac{1}{n}\sum_{i=1}^{n}|y_i - \hat{y}_i|$$

$$NMAE = \frac{1}{n}\sum_{i=1}^{n}\left|\frac{y_i - \hat{y}_i}{y_i}\right|$$

$$MBE = \frac{1}{n}\sum_{i=1}^{n}(\hat{y}_i - y_i)$$

The 95% confidence intervals have been calculated for estimating the coefficients of the three models, and they are all significant. Although the CFTool used previously for adjusting the flame height Eq. (5) can be used for Eqs. (31) and (32), it cannot be used for Eq. (33) because it depends on three variables: FMC, wind speed, and terrain slope. CFTool provides a flexible interface for fitting curves and surfaces to data, but not for more than two independent variables. The use of the `lsqcurvefit` function is more flexible for computing the error metrics, and upholds uniformity in the analysis of the three models. PhyFire states all data in SI units, although in the fitting of Eqs. (31), (32) and (33), ROS has been measured in m min^{-1}, as in the literature reviewed, for obtaining values of the exponential coefficient k comparable to those found in the references. FMC is measured in %, and wind speed in m s^{-1}.

Table 5
Statistical measures of performance for Eq. (31) fitted with PhyFire data ($n = 17$). ROS: rate of spread; k: exponential coefficient; FMC: fuel moisture content; R^2: coefficient of determination; R^2_{Adj}: coefficient of determination adjusted to degrees of freedom; RMSE: root-mean-square error; NRMSE: normalized root-mean-square error; MAE: mean absolute error; NMAE: normalized mean absolute error; MBE: mean bias error.

Eq. (31) $ROS = c\, e^{-k\,FMC}$ Slope: 20%, Wind: 20 km h^{-1} (mean values)

	k	R^2	R^2_{Adj}	RMSE	NRMSE	MAE	NMAE	MBE
Fuel 1	0.0057	0.8856	0.8779	2.728	0.1030	2.205	0.0925	−0.1184
	(0.005)	(0.831)	(0.819)	(2.296)	(0.0965)	(1.908)	(0.0947)	(−0.110)
Fuel 4	0.0059	0.8858	0.8782	2.669	0.1040	2.252	0.1002	−0.1455
	(0.0057)	(0.836)	(0.826)	(2.478)	(0.1211)	(2.144)	(0.1193)	(−0.132)
Fuel 5	0.0034	0.7544	0.7380	1.150	0.1060	1.306	0.0970	−0.0309
	(0.0035)	(0.773)	(0.758)	(1.364)	(0.0963)	(1.189)	(0.9255)	(−0.044)
Fuel 6	0.0051	0.8104	0.7977	2.235	0.1235	2.016	0.1234	−0.0999
	(0.0050)	(0.811)	(0.799)	(1.954)	(0.1168)	(1.674)	(0.1124)	(−0.094)
Fuel 7	0.0055	0.8303	0.8290	2.309	0.1212	2.088	0.1240	−0.1179
	(0.0050)	(0.815)	(0.802)	(1.973)	(0.1165)	(1.690)	(0.1119)	(−0.097)
Mean	0.0048	0.8131	0.8006	2.009	0.1096	1.719	0.1063	−0.0953

Table 6
Statistical measures of performance for Eq. (32) fitted with PhyFire data ($n = 17$). ROS: rate of spread; c, b, k: model coefficients; FMC: fuel moisture content; R^2: coefficient of determination; R^2_{Adj}: coefficient of determination adjusted to degrees of freedom; RMSE: root-mean-square error; NRMSE: normalized root-mean-square error; MAE: mean absolute error; NMAE: normalized mean absolute error; MBE: mean bias error. The three values of each cell correspond to each slope, 0%, 20%, and 40%, respectively.

Eq. (32) $ROS = c\, v^b\, e^{-k\,FMC}$ Slope: 0% − 20% − 40%.

Fuel	c	b	k	R^2	R^2_{Adj}	RMSE	NRMSE	MAE	NMAE	MBE
1	0.406	2.297	0.006	0.889	0.886	3.224	0.233	2.703	0.263	−0.604
	1.175	2.104	0.006	0.920	0.917	5.431	0.191	4.558	0.216	−0.809
	6.722	1.424	0.003	0.926	0.924	7.584	0.137	6.009	0.133	−0.122
4	5.134	0.718	0.005	0.902	0.899	1.606	0.146	1.282	0.130	−0.062
	8.865	0.797	0.006	0.928	0.926	2.796	0.136	2.347	0.141	−0.239
	12.78	0.954	0.005	0.963	0.962	4.078	0.106	3.313	0.109	−0.208
5	2.743	0.679	0.001	0.920	0.918	0.675	0.103	0.562	0.098	−0.004
	6.038	0.618	0.003	0.924	0.901	1.415	0.119	1.138	0.099	−0.046
	11.59	0.597	0.005	0.881	0.878	3.016	0.128	2.519	0.140	−0.164
6	3.859	0.705	0.003	0.914	0.912	1.007	0.124	0.880	0.116	−0.006
	6.650	0.782	0.005	0.874	0.871	2.679	0.171	0.878	0.063	−0.006
	12.78	0.751	0.006	0.932	0.930	3.612	0.128	3.019	0.132	−0.279
7	3.752	0.727	0.003	0.918	0.916	1.079	0.124	0.880	0.114	−0.008
	7.345	0.740	0.005	0.887	0.884	2.566	0.158	2.033	0.149	−0.193
	13.49	0.731	0.006	0.935	0.933	3.505	0.124	2.927	0.126	−0.250

5. Results and discussion

The exponential relationship between ROS and FMC described by Eq. (31) explains on average 80% of the cases in all the scenarios, with better results in cases with steeper slopes and higher wind speeds. Table 5 shows fitted values and all the metrics computed to assess the goodness of fit for each one of the five fuel types and an intermediate scenario of 20% slope and 20 km h^{-1} wind speed. No significant differences are observed between the chosen intermediate scenario and the mean values of all scenarios. All the fuels record a similar performance, with fuel 5 having a worse R^2 but better MAE. The negative but small values of the MBE imply that the model slightly underestimates ROS. Values of pre-exponential factor c are not shown because they vary considerably depending on wind speed and terrain slope, as expected. The pre-exponential factor of Eqs. (32) and (33) reflects this behavior. Fig. 1 shows the predicted ROS values for all the fuel types and the scenario selected for Table 5, namely, 20% terrain slope and 20 km h^{-1} wind speed. The behavior of the different types of fuels can be appreciated. ROS values are in full agreement with the photo-guide data Arellano et al. (2016).

Eq. (32) incorporates the effect of wind speed, achieving a better fit, explaining on average 90% of cases for all the slopes and fuel types in terms of R^2 and also R^2_{Adj}, so the improvement in fit cannot be attributed to increased degrees of freedom. RMSE and MAE increase with the slope, but this is due to higher values of ROS. However, the normalized versions of these error measures, NRMSE and NMAE, remain in the same range for all slopes and fuel types. Table 6 shows fitted values and all the metrics computed.

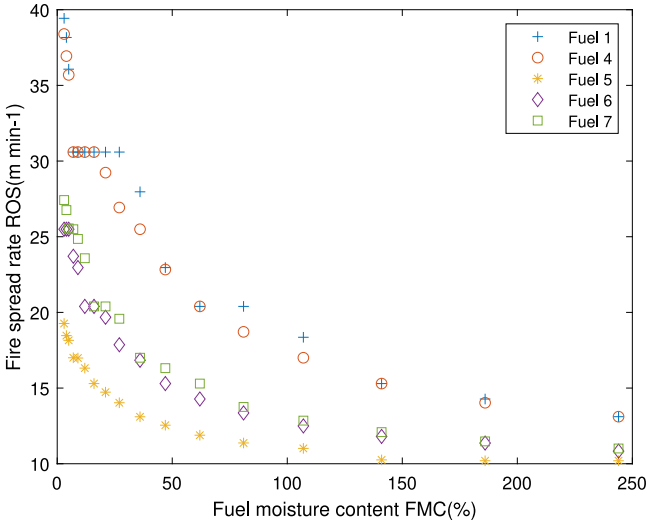

Fig. 1. Relationship between ROS (m min^{-1}) PhyFire calculations and FMC for all the fuel types analyzed corresponding to a scenario of 20% terrain slope and 20 km h^{-1} wind speed.

Table 7
Statistical measures of performance for Eq. (33) fitted with PhyFire data ($n = 17$). ROS: rate of spread; c, b, p, k: model coefficients; FMC: fuel moisture content; R^2: coefficient of determination; R^2_{Adj}: coefficient of determination adjusted to degrees of freedom; RMSE: root-mean-square error; NRMSE: normalized root-mean-square error; MAE: mean absolute error; NMAE: normalized mean absolute error; MBE: mean bias error.

Eq. (33) $ROS = c\, e^{p\, s - k\, FMC}$

Fuel	c	b	p	k	R^2	R^2_{Adj}	RMSE	NRMSE	MAE	NMAE	MBE
1	1.472	1.577	3.172	0.004	0.940	0.9406	6.529	0.201	4.784	0.188	0.208
4	3.805	0.908	3.231	0.006	0.970	0.970	3.118	0.134	2.470	0.141	−0.297
5	3.504	0.606	2.904	0.004	0.936	0.935	3,105	0.161	1.538	0.128	−0.109
6	3.854	0.754	2.995	0.006	0.951	0.950	2.737	0.156	2.078	0.144	−0.236
7	4.103	0.733	2.949	0.006	0.954	0.954	2.658	0.150	2.024	0.139	−0.199

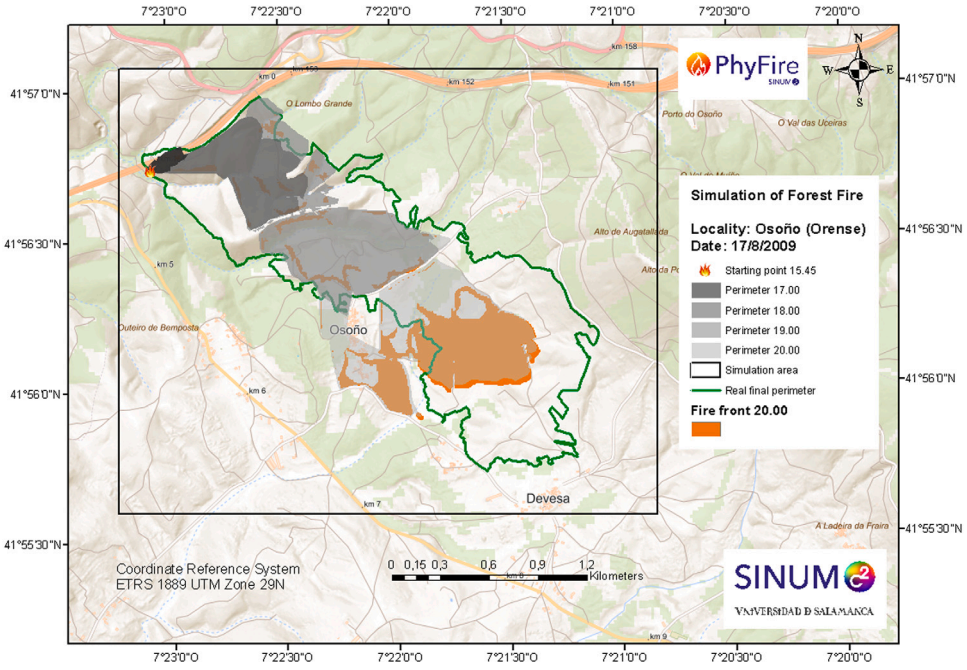

Fig. 2. Simulated burned areas each hour and fire front at 20.00 considering the simulation area defined by the black rectangle. Fire ignition point and real final perimeter were reported by the fire-suppression team.

Finally, Eq. (33), which also incorporates the effect of the slope, achieves an optimal fit, with $R^2_{Adj} > 0.95$ for almost all the fuel types, except grassland (fuel type 1) with $R^2_{Adj} > 0.94$, probably due to fewer data, and fuel type 5 ($R^2_{Adj} > 0.936$), the worst performing brush in all the settings, as can be seen in Table 6. Coefficients p and k, reflecting the effect of slope and FMC, respectively, record similar values for all the fuels, as in the experimental cases appearing in the Refs. (Fernandes et al., 2009). The exponential coefficient of wind term records a similar value for grassland (fuel type 1) and brush, as well as the pre-exponential factor c, which is explained by the different fire behavior of grasslands and brushlands. The normalized versions of the error measures, NRMSE and NMAE, maintain acceptable values, as does MBE. Eq. (33) slightly overestimates the ROS for grassland (fuel type 1), and slightly underestimates the ROS for brushlands (see Table 7).

Eq. (31) is fulfilled for several fuel types, wind speeds, and terrain slopes, and the value of the coefficient k obtained also remains within the same range for Eqs. (32) and (33), which considers wind and slope, and it is within the limits set by the studies that have evaluated it.

Certain discrepancies of a quantitative nature that can be observed in the values obtained for the exponential factor and the ROS, may be due to the fact that the model parameters have been adjusted based on the data available at Arellano et al. (2016), constrained to an FMC of 6%. The radiation absorption coefficient a can be sensitive to FMC, and wider flame length and ROS data would provide a more reliable fit of the model parameters and would reduce the observed discrepancies.

6. A real example

The real example used to illustrate this study occurred in an area of the autonomous region of Galicia, since the analysis carried out corresponds to fuels typical of this area of north-western Spain. This case has already been used in two previous publications (Prieto et al., 2017; Asensio et al., 2021), where details of the fire extension, the characteristics of the affected area and the meteorological conditions can be found. However, we summarize here the most relevant data. This wildfire occurred in Osoño (Orense), at 15:25 (local time) on August 17, 2009, burning 224 ha of Pinus pinaster, shrubland and grassland. Ambient temperature was above 30 °C and humidity below 30%. The wind was increasing from 2 m/s to almost 5 m/s. The fire developed during the afternoon, and in the areas most exposed to solar radiation (western face) the fire spread more rapidly. This is precisely the feature that we have sought to capture with this new simulation, the fuel in areas more exposed to solar radiation has lower moisture content and this affects the fire behavior in these areas.

We have simulated four different scenarios: taking into account some of the actions of the firefighting teams, in particular three large firebreaks on the right flank, without these actions, with a constant FMC throughout the simulation domain, and with a variable FMC depending on the solar radiation received, reducing it by 5% in the west-facing areas. The simulation of each scenario involved about 150 s of computing time on a laptop computer equipped with an Intel i7 processor (dual-core, 3.50 GHz) and 16 GB of RAM, for a rectangular

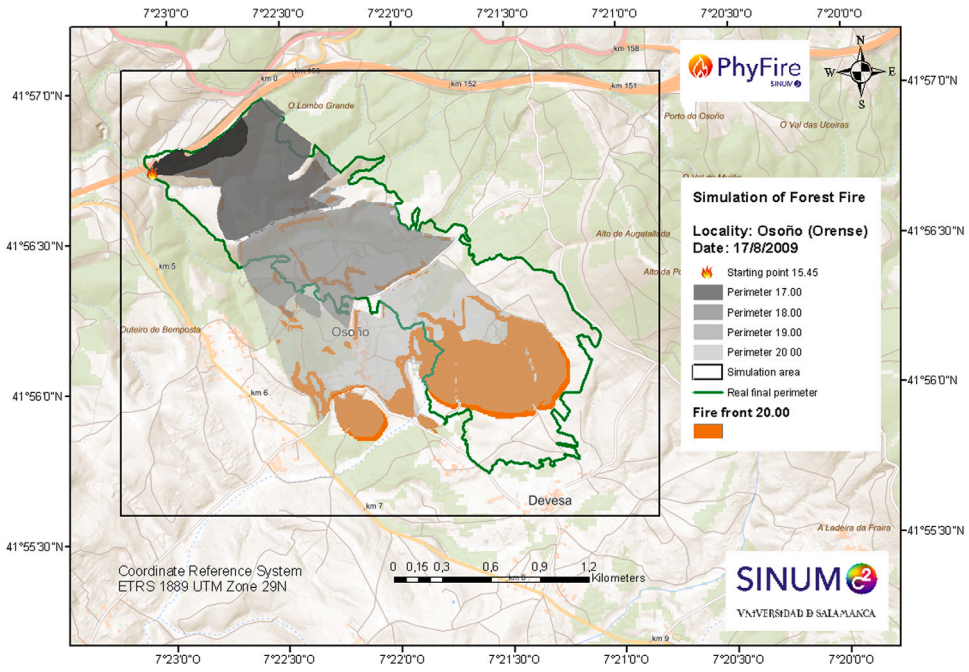

Fig. 3. Simulated burned areas each hour and fire front at 20.00 considering the simulation area defined by the black rectangle. FMC was reducing by 5% in the west-facing areas.

simulation area of 3320 m × 2745 m and a resolution of 7.5 m for the finite element mesh.

Fig. 2 shows the result of the simulation with the PhyFire model of the Osoño fire during the first four and a quarter hours, assuming that the fuel moisture is spatially uniform and without considering the actions of the firefighting teams. In Fig. 3, we have considered the effect of solar radiation on the west-facing areas, reducing humidity by 5%, which shows how the fire advances more rapidly and affects a larger area in these areas. Fig. 4 shows how the fire lines designed by the firefighters were effective in preventing the fire from reaching the nearby population even in the worst case scenario in terms of FMC. This scenario is consistent with the report of the firefighting teams, which designed three firebreaks to prevent the fire from reaching the nearest population. Nevertheless, the actions of the fire truck water tanks on flanks during the last part of the fire, were not considered in the simulation. This may explain why our simulation exceeds the perimeter.

7. Summary and conclusions

This study has explored the sensitivity of fire ROS and certain environmental conditions, mainly FMC, but also wind speed and terrain slope, in numerical simulations performed by the simplified physical PhyFire model. The results are qualitatively compared to field and tunnel-based experiments and with others numerical experiments found in the literature. The conclusion is that the PhyFire model is highly consistent with an exponential decay of fire ROS compared to FMC alone, and also in the presence of wind speed and terrain slope. PhyFire therefore performs as expected with respect to FMC according to the experimental models reviewed, with a high degree of accuracy in all the scenarios analyzed. This study therefore proves that the innovative and original way in which PhyFire considers the effect of FMC through a multivalued operator is highly significant. We have also observed the existence of an FMC threshold above which the response of ROS to increasingly higher FMC is weak, as in the experimental studies. Overall, this work shows the expediency of studying specific aspects of complex simulation models to improve their understanding with a view to increasing their overall efficiency. The development of wildland fire simulation models is a very complex task and their applicability is a matter of discussion (Alexander and Cruz, 2013). One way to tackle this challenge is to conduct a detailed analysis of specific aspects that allow for the model's overall improvement. Updated information on time and space for FMC will provide better simulation results, as evidenced by the real fire simulation. Therefore, in order to improve the accuracy of fire spread simulation, it would be highly desirable to use all the technology and new methods at our disposal to enhance the FMC information (Sharples et al., 2009; Miller et al., 2022; Quan et al., 2017).

Software availability

Name of the software: PhyFire. Developer: Luis Ferragut, M. Isabel Asensio, J. Manuel Cascón, Diego Prieto. Contact information: sinumcc@usal.es Program language: C++, Neptno++, OpenMP. Software availability: http://sinumcc.usal.es/

Declaration of competing interest

The authors declare that they have no known competing financial interests or personal relationships that could have appeared to influence the work reported in this paper.

Data availability

Data will be made available on request.

Acknowledgments

This research has been partially supported by the Spanish Ministry of Economy and Competitiveness (MINECO) through project PID2019-107685RB-I00, the European Regional Development Fund (ERDF), the Department of Education of the regional government, the Junta de Castilla *y* León, Spain (grant contract SA089P20), and the European Union's Horizon 2020 - Research and Innovation Framework Programme under grant agreement ID 101036926.

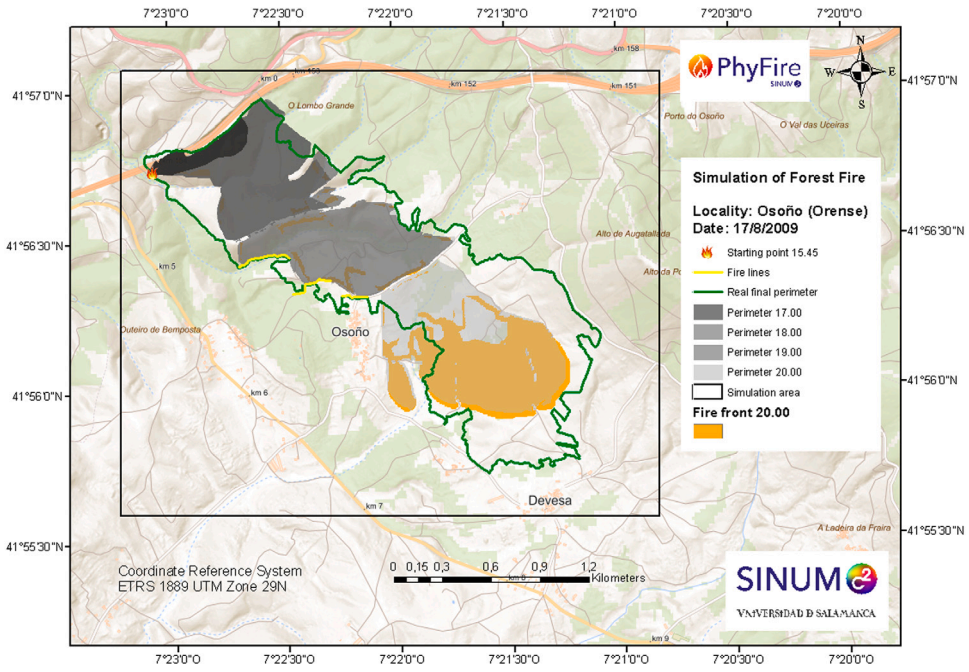

Fig. 4. Simulated burned areas each hour and fire front at 20.00 considering the simulation area defined by the black rectangle. Reduced FMC and three fire lines designed by the fire-suppression team (yellow lines) were considered.

References

Albini, F., 1976. Estimating Wildfire Behavior and Effects. Gen. Tech. Rep. INT-GTR-30, USDA Forest Service, Intermountain Forest and Range Experiment Station, Ogden, UT, URL https://www.fs.usda.gov/research/treesearch/29574.

Alexander, M.E., Cruz, M.G., 2013. Are the applications of wildland fire behaviour models getting ahead of their evaluation again? Environ. Model. Softw. 41, 65–71. http://dx.doi.org/10.1016/j.envsoft.2012.11.001.

Álvarez, D., Prieto, D., Asensio, M.I., Cascón, J.M., Ferragut, L., 2017. Parallel implementation of a simplified semi-physical wildland fire spread model using OpenMP. In: Martínez de Pisón, F.J., Urraca, R., Quintián, H., Corchado, E. (Eds.), Hybrid Artificial Intelligent Systems. Springer International Publishing, Cham, pp. 256–267, URL https://link.springer.com/chapter/10.1007/978-3-319-59650-1_22.

Anderson, H., 1982. Aids to Determining Fuel Models for Estimating Fire Behavior. Technical Report, USDA Forest Service, Ogden, UT, http://dx.doi.org/10.2737/INT-GTR-122.

Anderson, W., Cruz, M., Fernandes, P., McCaw, L., Vega, J., Bradstock, R., Fogarty, L., Gould, J., McCarthy, G., Marsden-Smedley, J., Matthews, S., Mattingley, G., Pearce, H., van Wilgen, B., 2015. A generic, empirical-based model for predicting rate of fire spread in shrublands. Int. J. Wildland Fire 24, 443–460. http://dx.doi.org/10.1071/WF14130.

Arellano, S., Vega, J., Ruíz, A., Arellano, A., Álvarez, J., Vega, D., E, P., 2016. Foto-guía de Combustibles Forestales De Galicia. Versión I. Andavira Editora SL, Santiago de Compostela, Spain.

Asensio, M.I., Cascón, J.M., Prieto-Herráez, D., Ferragut, L., 2023. An historical review of the simplified physical fire spread model PhyFire: Model and numerical methods. Appl. Sci. 13 (4), http://dx.doi.org/10.3390/app13042035.

Asensio, M.I., Ferragut, L., Álvarez, D., Laiz, P., Cascón, J.M., Prieto, D., Pagnini, G., 2021. PhyFire: An online GIS-integrated wildfire spread simulation tool based on a semiphysical model. In: Asensio, M.I., Oliver, A., Sarrate, J. (Eds.), Applied Mathematics for Environmental Problems. Springer International Publishing, Cham, pp. 1–20.

Asensio, M., Ferragut, L., Simon, J., 2005. A convection model for fire spread simulation. Appl. Math. Lett. 18 (6), 673–677. http://dx.doi.org/10.1016/j.aml.2004.04.011.

Asensio-Sevilla, M., Santos-Martín, M., Álvarez-León, D., Ferragut-Canals, L., 2020. Global sensitivity analysis of fuel-type-dependent input variables of a simplified physical fire spread model. Math. Comput. Simulation 172, 33–44. http://dx.doi.org/10.1016/j.matcom.2020.01.001.

Bermúdez, A., Moreno, C., 1981. Duality methods for solving variational inequalities. Comput. Math. Appl. 7 (1), 43–58. http://dx.doi.org/10.1016/0898-1221(81)90006-7.

Burrows, N., 1999. Fire behaviour in jarrah forest fuels: 2. Field experiments. CALMScience 3 (1), 57–84.

Cardil, A., Monedero, S., Schag, G., de Miguel, S., Tapia, M., Stoof, C.R., Silva, C.A., Mohan, M., Cardil, A., Ramirez, J., 2021. Fire behavior modeling for operational decision-making. Curr. Opin. Environ. Sci. Health 23, 100291. http://dx.doi.org/10.1016/j.coesh.2021.100291.

Cascón, J., Ferragut, L., Asensio, M., Prieto, D., Álvarez, D., 2018. Neptuno ++: An adaptive finite element toolbox for numerical simulation of environmental problems. In: XVIII Spanish- French School Jacques-Louis Lions About Numerical Simulation in Physics and Engineering. Las Palmas de Gran Canaria.

Chapman, B., Jost, G., Van Der Pas, R., 2007. Using OpenMP: Portable Shared Memory Parallel Programming. MIT Press. Cambridge.

Cheney, N., Gould, J., Catchpole, W., 1993. The influence of fuel, weather and fire shape variables on fire-spread in grasslands. Int. J. Wildland Fire 3 (1), 31–44. http://dx.doi.org/10.1071/WF9930031.

Chuvieco, E., González, I., Verdú, F., Aguado, I., Yebra, M., 2009. Prediction of fire occurrence from live fuel moisture content measurements in a Mediterranean ecosystem. Int. J. Wildland Fire 18 (4), 430–441. http://dx.doi.org/10.1071/WF08020.

Cox, G., 1995. Combustion Fundamentals of Fire. Academic Press, New York.

Ellis, T., Bowman, D., Piyush, J., Flannigan, M., Williamson, G., 2022. Global increase in wildfire risk due to climate-driven declines in fuel moisture. Global Change Biol. 28 (4), e1760. http://dx.doi.org/10.1111/gcb.16006.

Fernandes, P., Botelho, H., Rego, F., Loureiro, C., 2009. Empirical modelling of surface fire behaviour in maritime pine stands. Int. J. Wildland Fire 18, 698–710. http://dx.doi.org/10.1071/WF08023.

Ferragut, L., Asensio, M.I., Cascón, J.M., Prieto, D., 2015. A wildland fire physical model well suited to data assimilation. Pure Appl. Geophys. 172 (1), 121–139. http://dx.doi.org/10.1007/s00024-014-0893-9.

Ferragut, L., Asensio, M., Cascón, J., Prieto, D., Ramírez, J., 2013. An efficient algorithm for solving a multi-layer convection-diffusion problem applied to air pollution problems. Adv. Eng. Softw. 65, 191–199. http://dx.doi.org/10.1016/j.advengsoft.2013.06.010.

Ferragut, L., Asensio, M., Monedero, S., 2007. A numerical method for solving convection-reaction-diffusion multivalued equations in fire spread modelling. Adv. Eng. Softw. 38 (6), 366–371. http://dx.doi.org/10.1016/j.advengsoft.2006.09.007.

Ferragut, L., Asensio, M., Simon, J., 2011. High definition local adjustment model of 3D wind fields performing only 2D computations. Int. J. Numer. Methods Biomed. Eng. 27 (4), 510–523. http://dx.doi.org/10.1002/cnm.1314.

Finney, M., Cohen, J., McAllister, S., Jolly, W., 2013. On the need for a theory of wildland fire spread. Int. J. Wildland Fire 22 (1), 25–36. http://dx.doi.org/10.1071/WF11117.

Group, F.C.F.D., 1992. Development and Structure of the Canadian Forest Fire Behavior Prediction System. Information Report ST-X-3, Forestry Canada, Science and Sustainable Development Directorate, Ottawa, ON, URL https://d1ied5g1xfgpx8.cloudfront.net/pdfs/10068.pdf.

Lopes, A., Cruz, M., Viegas, D., 2002. FireStation — An integrated software system for the numerical simulation of fire spread on complex topography. Environ. Model. Softw. 17 (3), 269–285. http://dx.doi.org/10.1016/S1364-8152(01)00072-X.

Mandel, J., Beezley, J.D., Kochanski, A.K., 2011. Coupled atmosphere-wildland fire modeling with WRF 3.3 and SFIRE 2011. Geosci. Model Dev. 4 (3), 591–610. http://dx.doi.org/10.5194/gmd-4-591-2011.

Marino, E., Dupuy, J.-L., Pimont, F., Guijarro, M., Hernando, C., Linn, R., 2012. Fuel bulk density and fuel moisture content effects on fire rate of spread: a comparison between FIRETEC model predictions and experimental results in shrub fuels. J. Fire Sci. 30 (4), 277–299. http://dx.doi.org/10.1177/0734904111434286.

Mell, W.E., Jenkins, M.A., Gould, J.S., Cheney, P.B., 2007. A physics-based approach to modelling grassland fires. Int. J. Wildland Fire 16, 1–22. http://dx.doi.org/10.1071/WF06002.

Miller, L., Zhu, L., Yebra, M., Rüdiger, C., Webb, G.I., 2022. Multi-modal temporal CNNs for live fuel moisture content estimation. Environ. Model. Softw. 156, 105467. http://dx.doi.org/10.1016/j.envsoft.2022.105467.

Morvan, D., 2011. Physical phenomena and length scales governing the behaviour of wildfires: A case for physical modelling. Fire Technol. 47, 437–460. http://dx.doi.org/10.1007/s10694-010-0160-2.

Morvan, D., 2013. Numerical study of the effect of fuel moisture content (FMC) upon the propagation of a surface fire on a flat terrain. Fire Saf. J. 58, 121–131. http://dx.doi.org/10.1016/j.firesaf.2013.01.010.

Papadopoulos, G.D., Pavlidou, F.-N., 2011. A comparative review on wildfire simulators. IEEE Syst. J. 5 (2), 233–243. http://dx.doi.org/10.1109/JSYST.2011.2125230.

Pianosi, F., Sarrazin, F., Wagener, T., 2015. A matlab toolbox for global sensitivity analysis. Environ. Model. Softw. 70, 80–85. http://dx.doi.org/10.1016/j.envsoft.2015.04.009.

Prieto, D., Asensio, M., Ferragut, L., Cascón, J., 2015. Sensitivity analysis and parameter adjustment in a simplified physical wildland fire model. Adv. Eng. Softw. 90, 98–106. http://dx.doi.org/10.1016/j.advengsoft.2015.08.001.

Prieto, D., Asensio, M., Ferragut, L., Cascón, J., Morillo, A., 2017. A GIS-based fire spread simulator integrating a simplified physical wildland fire model and a wind field model. Int. J. Geogr. Inf. Sci. 1–22. http://dx.doi.org/10.1080/13658816.2017.1334889.

Prieto-Herráez, D., Frías-Paredes, L., Cascón, J., Lagüela-López, S., Gastón-Romeo, M., Asensio-Sevilla, M., Martín-Nieto, I., Fernandes-Correia, P., Laiz-Alonso, P., Carrasco-Díaz, O., Sáez-Blázquez, C., Hernández, E., Ferragut-Canals, L., González-Aguilera, D., 2021. Local wind speed forecasting based on WRF-HDWind coupling. Atmos. Res. 248, 105219. http://dx.doi.org/10.1016/j.atmosres.2020.105219.

Quan, X., He, B., Yebra, M., Yin, C., Liao, Z., Li, X., 2017. Retrieval of forest fuel moisture content using a coupled radiative transfer model. Environ. Model. Softw. 95, 290–302. http://dx.doi.org/10.1016/j.envsoft.2017.06.006.

Rossa, C., Fernandes, P., 2017. Fuel-related fire-behaviour relationships for mixed live and dead fuels burned in the laboratory. Can. J. Forest Res. 47 (7), http://dx.doi.org/10.1139/cjfr-2016-0457.

Rossa, C., Fernandes, P., 2018a. On the fire-spread rate influence of some fuel bed parameters derived from Rothermel's model thermal energy balance. Šumarski List 142 (1–2), 77–88. http://dx.doi.org/10.31298/sl.142.1-2.7.

Rossa, C., Fernandes, P., 2018b. Short communication: On the effect of live fuel moisture content on fire-spread rate. Forest Syst. 26 (3), eSC08. http://dx.doi.org/10.5424/fs/2017263-12019.

Rossa, C., Veloso, R., Fernandes, P., 2016. A laboratory-based quantification of the effect of live fuel moisture content on fire spread rate. Int. J. Wildland Fire 25, 569–573. http://dx.doi.org/10.1071/WF15114.

Rothermel, R., 1972. A Mathematical Model for Predicting Fire Spread in Wildland Fuels. Res. Pap. INT-115, USDA Forest Service, Intermountain Forest and Range Experiment Station, Ogden, UT, URL https://www.fs.usda.gov/research/treesearch/32533.

Saltelli, A., Ratto, M., Andres, T., Campolongo, F., Cariboni, J., Gatelli, D., Saisana, M., Tarantola, S., 2008. Global sensitivity analysis. In: The Primer. John Wiley & Sons Ltd, http://dx.doi.org/10.1002/9780470725184.

Sharples, J., McRae, R., Weber, R., Gill, A., 2009. A simple index for assessing fuel moisture content. Environ. Model. Softw. 24 (5), 637–646. http://dx.doi.org/10.1016/j.envsoft.2008.10.012.

Stocks, B.J., Lawson, B.D., Alexander, M.E., Wagner, C.E.V., McAlpine, R.S., Lynham, T.J., Dubé, D.E., 1989. Canadian forest fire danger rating system: An overview. For. Chron. 65 (4), 258–265. http://dx.doi.org/10.5558/tfc65258-4.

Sullivan, A.L., 2009a. Wildland surface fire spread modelling, 1990 - 2007. 1: Physical and quasi-physical models. Int. J. Wildland Fire 18 (4), 349. http://dx.doi.org/10.1071/WF06143.

Sullivan, A.L., 2009b. Wildland surface fire spread modelling, 1990 - 2007. 2: Empirical and quasi-empirical models. Int. J. Wildland Fire 18 (4), 369. http://dx.doi.org/10.1071/WF06142.

Viegas, D., Soares, J., Almeida, M., 2013. Combustibility of a mixture of live and dead fuel components. Int. J. Wildland Fire 22, 992–1002. http://dx.doi.org/10.1071/WF12031.

Vilar, L., Herrera, S., Tafur-García, E., Yebra, M., Martínez-Vega, J., Echavarría, P., Martín, M., 2021. Modelling wildfire occurrence at regional scale from land use/cover and climate change scenarios. Environ. Model. Softw. 145, 105200. http://dx.doi.org/10.1016/j.envsoft.2021.105200.

Yebra, M., Dennison, P.E., Chuvieco, E., Riaño, D., Zylstra, P., Hunt, E.R., Danson, F.M., Qi, Y., Jurdao, S., 2013. A global review of remote sensing of live fuel moisture content for fire danger assessment: Moving towards operational products. Remote Sens. Environ. 136, 455–468. http://dx.doi.org/10.1016/j.rse.2013.05.029.

Yoo, S., Song, J., 2023. Rapid prediction of wildfire spread using ensemble Kalman filter and polyline simplification. Environ. Model. Softw. 160, 105610. http://dx.doi.org/10.1016/j.envsoft.2022.105610.